IOP PUBLISHING NANOTECHNOLOGY
Nanotechnology **18** (2007) 315603 (6pp) doi:10.1088/0957-4484/18/31/315603

Quantum dots by ultraviolet and x-ray lithography

Massimo F Bertino[1,7], Raghuveer R Gadipalli[1], Lane A Martin[1], Lauren E Rich[1], Alexey Yamilov[1], Brian R Heckman[2], Nicholas Leventis[3,7], Suchi Guha[4], John Katsoudas[5], Ralu Divan[6] and Derrick C Mancini[6]

[1] Department of Physics, University of Missouri-Rolla, MO 65409, USA
[2] Midwest Research Institute, 425 Volker Boulevard, Kansas City, MO 64110, USA
[3] Department of Chemistry, University of Missouri-Rolla, MO 65409, USA
[4] Department of Physics, University of Missouri-Columbia, Columbia, MO 65211, USA
[5] Center for Synchrotron Radiation Research and Instrumentation, Illinois Institute of Technology, Chicago, IL 60616, USA
[6] Center for Nanoscale Materials, Argonne National Laboratory, 9700 S. Cass Avenue, Building 440 Room A130, Argonne, IL 60439-4812, USA

E-mail: Massimo@umr.edu and leventis@umr.edu

Received 22 February 2007, in final form 7 May 2007
Published 6 July 2007
Online at stacks.iop.org/Nano/18/315603

Abstract
Highly luminescent semiconductor quantum dots have been synthesized in porous materials with ultraviolet and x-ray lithography. For this, the pore-filling solvent of silica hydrogels is exchanged with an aqueous solution of a group II metal ion together with a chalcogenide precursor such as 2-mercaptoethanol, thioacetamide or selenourea. The chalcogenide precursor is photodissociated in the exposed regions, yielding metal chalcogenide nanoparticles. Patterns are obtained by using masks appropriate to the type of radiation employed. The mean size of the quantum dots is controlled by adding capping agents such as citrate or thioglycerol to the precursor solution, and the quantum yield of the composites can be increased to up to about 30% by photoactivation. Our technique is water-based, uses readily available reagents, and highly luminescent patterned composites are obtained in a few simple processing steps. Polydispersity, however, is high (around 50%), preventing large-scale usage of the technique for the time being. Future developments that aim at a reduction of the polydispersity are presented.

1. Introduction

In the last few years, a wide array of quantum dot-based devices and composites has been proposed for applications ranging from nonlinear optics [1–4] to light emitting diodes [5, 6], sensors [7–9], and lasers [10–12]. Large-scale use of these devices and materials, however, is limited by cost and manufacturing issues. It was recognized early that applications could be made more readily available if quantum dots could be synthesized with bottom-up techniques which are compatible with conventional microfabrication methods such as photolithography [13]. However, progress in this direction has been sluggish. Only very recently, patterning of substrates with quantum dots was reported, and it was obtained with a top-down approach; photocorrosion of films of pre-formed quantum dots [14].

We recently demonstrated that quantum dots can be synthesized in selected regions of porous matrices by photodissociation of appropriate precursors. In the first demonstration of our photolithographic technique the precursors were dissociated thermally by focused infrared light (IR) [15, 16]. Heat diffusion, however, rendered the use of masks impractical. Only relatively primitive patterns could be produced by translating the sample in front of the focused

[7] Authors to whom any correspondence should be addressed.

beam. We then showed that ultraviolet light (UV) can also be employed to pattern substrates with quantum dots [17]. However, photodissociation of the thiol precursors employed in the UV experiments was not very efficient. The incident light had to be tightly focused, and patterns could be produced only by translating the sample in front of a small illuminated spot, as in the IR case. In addition, the composites produced with both IR and UV lithographies had a very low quantum yield of below 1%. Here we expand those methods and we show that: (i) photodissociation can be made more efficient by using a different set of precursors, allowing production of complex patterns by masking; (ii) the quantum yield of the composites can be increased to up to about 30% by photoactivation; (iii) quantum dots can be produced with x-ray lithography. Our quantum dot photolithography (QDPL) technique has therefore come a long way and includes several attractive features, each of which has deep implications for applications. For example, we now have precursor combinations that are easily photodissociated. Thus, it may be possible to use conventional ultraviolet exposure and masking tools to produce quantum dots. The high quantum yield of the composites, combined with their porosity, may allow applications of the materials as optical materials and sensors. X-ray lithography paves the way to ultra-high spatial resolution. In our experiments, comparatively hard x-rays (8.5 keV) were employed, for which masks can be realized which have a resolution of tens of microns. However, it is conceivable that soft x-rays could be employed, for which masks can be fabricated with a resolution of well below 1 μm [18]. We have also observed that features produced with x-ray lithography penetrated into the bulk of the monoliths for as much as 12 mm. These structures have an aspect ratio of around 200 and could conceivably be employed as waveguides. In fact, materials such as PbS have a much higher index of refraction ($n = 4.1$) than the matrix ($n = 1.1$–1.5) for silica gels. The addition of PbS in a concentration as little as 0.1% by volume to a silica gel increases the index of refraction of the composite by $\Delta n \approx 5 \times 10^{-3}$, which is sufficient for waveguiding applications. The main drawback of the technique, at this point, is probably polydispersity, which was estimated to be around 50% from the FWHM (full width at half maximum) of the exciton peak in the absorption spectra. Polydispersity might be eliminated by using matrices with well-contolled pore size, such as MCM-41 [19], or by size-selective photocorrosion [14, 20, 21], and this is where our research will focus in the near future.

2. Experimental details

2.1. Sample preparation

Silica hydrogels were prepared following a conventional base-catalyzed route [22]. The hydrogels were then washed several times in methanol and water. Hydrogel cylinders were then cut into smaller cylinders of about 7 mm in diameter and 5–7 mm in length. These cylinders were then immersed in 20 ml of a solution of a group II precursor and a group VI precursor. To produce CdS composites with ultraviolet photolithography, the precursor solution consisted of $Cd(NO_3)_2$ in a concentration of up to 0.5 mol l^{-1} (M) and thioacetamide (CH_3CSNH_2), or thiourea (H_2NCSNH_2), in concentrations of up to 0.5 M. The metal:sulfur mole ratio was kept at typically around 1:1. To produce CdSe composites with ultraviolet photolithography, the precursor solution consisted of $Cd(ClO_4)_2{\cdot}xH_2O$ ($x \sim 6$), in a concentration of up to 0.1 M, and selenourea ($H_2NCSeNH_2$), also in a concentration of up to 0.1 M. The metal:chalcogenide mole ratio was kept at typically around 4:1. The metal and the chalcogenide precursors tended to react at room temperature even without irradiation. To prevent the spontaneous formation of metal chalcogenides, a chelating agent such as triethanolamine was added to the precursor solution, in a concentration equal to that of the metal precursor. Alternatively, the vials containing the gels and the precursor solution were cooled to 5 °C. For x-ray lithography the bathing solution contained $Cd(NO_3)_2$ or $Pb(NO_3)_2$ in a concentration between 0.01 and 0.05 M. The chalcogenide source was 2-mercaptoethanol, in a typical concentration of 1 M. The precursor solutions for x-ray lithography were stable at room temperature, and cooling was not required. In all experiments, diffusion of the precursors inside the gels was usually complete within 2 h, at which point the gels were irradiated. The gels and bathing solution were kept under Ar during preparation and irradiation. Unreacted precursors were removed after exposure by placing the samples in a large volume (>100 ml) of cold water. This washing procedure was repeated three to four times. The particle size was controlled by adding a capping agent like citrate or 2-mercaptoethanol to the bathing solutions, in a concentration up to ten times higher than that of the metal ion.

2.2. Irradiation

Ultraviolet. The light source for ultraviolet photolithography was a high-pressure, 100 W Hg arc discharge lamp, whose light was collimated on the sample either with a long focal length lens or with a standard collimator system. Hydrogels filled with the precursor solution were placed in a quartz cuvette, filled with some of the solution for index matching, and placed in front of the beam. To prepare masks, a pattern was printed on paper with a laser printer, and a reduced copy was transferred on an acetate transparency with a standard copier. The mask was then placed on the outer surface of the cuvette, and the sample was irradiated.

X-ray. Irradiations were carried out at the Materials Research Collaborative Access Team (MRCAT) bending magnet beamline, at Argonne National Laboratory's Advanced Photon Source. The beamline has a beam-defining mask upstream of an 880 mm long in-vacuum platinum coated mirror held at an angle of 8 mrad used as a low-pass energy filter. The low-energy spectrum of the beamline is defined by the 375 μm thickness of the beryllium windows. The final dimensions of the collimated beam are approximately 100 mm by 6 mm. The beam was not monochromatic; the mean beam energy was 8.5 keV, and the FWHM of the energy distribution was around 6 keV. To prevent heating and damage to the gel structure, gels were translated in front of the beam at a typical speed of 20 mm s^{-1}. Hard x-ray masks for ultradeep x-ray lithography (UDXRL) were fabricated by electro-depositing a Au absorber layer with a thickness on the order of 50 μm on a thin (0.5 mm) graphite sheet. A detailed description of the mask fabrication procedure can be found in [23].

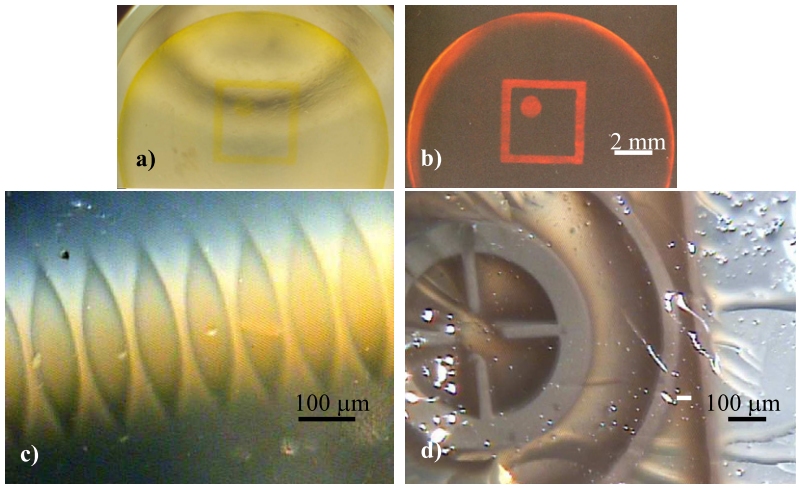

Figure 1. ((a), (b)) CdSe patterns obtained with UV lithography. (b) Photoluminescence of sample (a), obtained by illuminating the patterned sample with the 457.9 nm line of an Ar^+ laser. A laser goggle was interposed between the sample and the camera to filter the laser glare from the photoluminescence of the CdSe quantum dots. ((c), (d)) PbS patterns obtained with x-ray lithography.

(This figure is in colour only in the electronic version)

2.3. Characterization

Samples were characterized with ultraviolet–visible (UV–vis) optical absorption spectroscopy, photoluminescence spectroscopy, and Raman spectroscopy. Optical absorption spectra of hydrogel–quantum dot composites were taken with a CARY 5 ultraviolet–visible–near-infrared (UV–vis–NIR) spectrophotometer. Photoluminescence spectra were taken using a JY-Horiba Fluorolog 3-22 Fluorometer. Raman spectra were obtained using the 514.5 nm line of an Ar^+ laser and a SPEX 0.85 m double spectrometer equipped with a liquid N_2 cooled charge-coupled device array detector, or using a Renishaw micro-Raman spectrometer with a 785 nm excitation line. Due to the challenges of PbS Raman spectroscopy, a reference PbS powder was prepared separately. The powder was obtained by adding 0.1 M Na_2S to a 0.1 M $Pb(NO_3)_2$ solution. The precipitate was filtered and washed several times with water, methanol, and ethanol. The resulting powder was polydisperse, with grains varying from about 10 nm to a few microns.

2.4. Quantum yield measurements

Two different procedures were used to measure the quantum yield of the composites. In one case, a sample was illuminated with uncollimated UV light to originate a uniform distribution of semiconductor nanoparticles through the monolith. The emission of the composite was compared to that of a hydrogel which had the same dimensions of the composite, and where the solvent had been exchanged with a rhodamine solution. Alternatively, a CdSe spot with a diameter of about 1 mm was produced in a thin (about 1 mm) hydrogel. Exposure time and lens focal length were chosen such that the CdSe pattern penetrated through the sample, giving rise to a cylindrical feature. The sample was then illuminated through a mask which had the same diameter as the CdSe pattern, and the emission was compared to that of a rhodamine-loaded sample, illuminated through the same mask. For both procedures, the UV–vis spectrum of the composite and reference monolith were measured to account for differences in absorption. To rule out sample inhomogeneity and geometry issues, measurements were repeated for at least four composite samples prepared under the same conditions, and for four to five samples loaded with varying rhodamine concentrations.

3. Results and discussion

3.1. Pattern generation

Figure 1 shows sample patterns obtained by masking. Figure 1(a) shows a CdSe pattern obtained with UV photolithography. The image was taken under room lighting. Figure 1(b) shows the luminescence of the pattern in (a), excited by an Ar^+ laser. Figures 1(c) and (d) show PbS patterns obtained with x-ray lithography. For ease of representation, comparatively large patterns were produced. The resolution of the QDPL technique, however, is at least on the order of a few microns. A point resolution of about 3 μm was attained in our previous experiments by focusing an Ar ion laser beam on the surface of a gel with a low-magnification microscope objective. For the x-ray technique, a resolution on the order of 10 μm was obtained, which coincided with the fabrication limit of the x-ray mask [23].

3.2. Photodissociation and reaction mechanisms

Ultraviolet. The UV technique is based on the photodissociation of chalcogenide precursors. In our initial experiments, we employed a solution of Cd^{2+} and a thiol (RSH) like 2-mercaptoethanol [17]. Ultraviolet irradiation dissociated the thiols, yielding CdS. Photodissociation of these precursors, however, was not very efficient, and patterns could be created only by exposing matrices to tightly focused beams. In this work, we use different chalcogenide precursors which are also dissociated by UV light: thioacetamide, thiourea and

selenourea. The overall reaction scheme leading to chalcogenide nanoparticles is shown in equations (1) and (2) for thioacetamide [24]:

$$CH_3CSNH_2 + h\nu \rightarrow CH_3CN + H_2S \quad (1)$$

$$Cd^{2+} + H_2S \rightarrow CdS + 2H^+. \quad (2)$$

The use of selenourea as a source of selenium ions was investigated recently by other groups [25–27]. It was found that selenourea photodissociates easily, but care must be taken to avoid oxidation of Se^{2-} [27]. In our experiments, oxidation of the Se anions was prevented by the capping agents, citrate and thioglycerol, which are reducing agents.

The chalcogenide precursors employed in the present experiments were more easily photodissociated than the precursors used previously. In samples containing the same precursor concentration, clearly visible patterns were formed five to ten times more rapidly when selenourea was used instead of the 2-mercaptoethanol (RSH) used previously. In addition, the molar absorptivity at 254 nm (Hg line) of the Cd^{2+}–RSH precursor combination is 3.2×10^4 M^{-1} cm^{-1} [17]; the molar absorptivity of Cd^{2+}–selenourea is 1.0×10^4 M^{-1} cm^{-1}. When the differences in absorptivities and exposure times are taken into account, we obtain that UV irradiation of Cd^{2+}–selenourea is 15–30 times more efficient than that of Cd^{2+}–RSH.

X-ray. For x-ray lithography, the chalcogenide precursor was 2-mercaptoethanol. 2-mercaptoethanol is dissociated and liberates SH^- when it reacts with the solvated electrons and radicals liberated by the interaction of x-rays with water [28, 29]. The overall reaction leading to metal chalcogenides is reported in equations (3)–(5). Reduction of the metal ions by the solvated electrons, equation (6), was prevented by working in a large excess of thiol, typically 10–100 times the metal ion concentration:

$$H_2O + h\nu \rightarrow e^-_{(aq)}H^{\cdot}, OH^{\cdot}, H_3O^+, \ldots \quad (3)$$

$$HOCH_2CH_2SH + e^-_{(aq)} \rightarrow SH^- + {}^{\cdot}CH_2CH_2OH \quad (4)$$

$$SH^- + Pb^{2+} \rightarrow PbS + H^+ \quad (5)$$

$$Pb^{2+} + 2e^-_{(aq)} \rightarrow Pb^0. \quad (6)$$

Patterns were formed readily with x-ray lithography. Typically, an exposure to 85 mA min was sufficient to generate clearly visible patterns. This exposure is very low when compared to more conventional x-ray lithography processes such as LIthografie, Galvanoformung, Abformung (LIGA). These processes are usually based on radiation-induced cross-linking of polymers like poly(methyl metacrylate) (PMMA) which require extremely lengthy exposures. On our apparatus, PMMA structures were obtained after exposures on the order of 40 000 mA min. We also noticed that the chalcogenide patterns penetrated inside the gels for several millimetres, suggesting that x-ray lithography could be employed to fabricate three-dimensional quantum dot structures with a high aspect ratio.

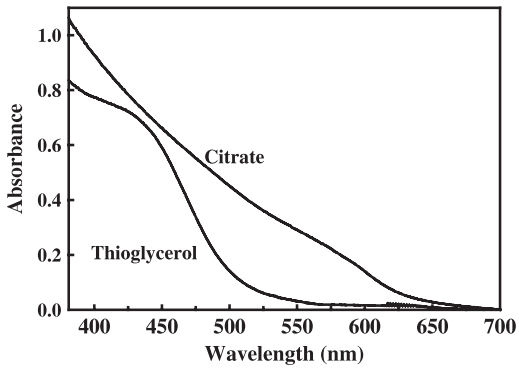

Figure 2. UV–vis absorption spectra of CdSe patterns produced with UV photolithography and the indicated capping agents in a concentration of 3.5×10^{-3} M. The parent solution contained 1.6×10^{-3} M cadmium perchlorate and 4×10^{-4} M selenourea.

3.3. Materials characterization

Semiconductor nanoparticles form within the exposed regions, and do not diffuse appreciably in the unexposed regions, at least within the limits of our measurements. The dimensions of the photolithographed features always coincided with those of the features on the masks, at least within the resolution of the optical microscope used for the measurements ($\sim$1 μm) [30]. The mean particle size was most efficiently controlled by adding capping agents to the precursor solution. The effect of capping agents on the mean particle size is shown in figure 2. CdSe samples capped with citrate exhibited an excitonic shoulder in the 570–580 nm range, which corresponds to a mean nanoparticle size of 5 nm [31]. Samples capped with a stronger capping agent such as thioglycerol exhibited an excitonic shoulder in the 430–440 nm range, corresponding to a mean nanoparticle size of 2.3 nm [32]. We point out, however, that the excitonic shoulders were always very broad, independent of the capping agent that we employed. The large FWHM of these shoulders is a clear indicator of polydispersity. In experiments from other groups, weak, undefined shoulders were associated with a $\sim$50% polydispersity, which is probably a realistic figure for our experiments [20]. We point out that size distribution histograms measured with transmission electron microscopy were not meaningful. In fact, for sizes below about 5 nm it is exceedingly difficult to distinguish the nanoparticles from density fluctuations of the silica matrix.

The as-grown composites were poorly luminescent, which is common for quantum dots grown in aqueous environment. The luminescence, however, could be increased considerably by photoactivation. For this, unreacted precursors were first washed out of the hydrogels. The samples were then exposed to a low-power ($\sim$15 W) black light. Light absorption by II–VI nanoparticles can induce oxidation of the chalcogenide, equation (7) [20, 31, 32]. Surface defects are photooxidized preferentially, thus photoactivation is a convenient way to remove such defects and improve the photoluminescence quantum yield [20, 21, 33–46].

$$CdSe + O_2 + h\nu \rightarrow Cd^{2+} + SeO_2. \quad (7)$$

Figure 3 reports the results of a typical photoactivation treatment of a CdSe-patterned sample. The emission of

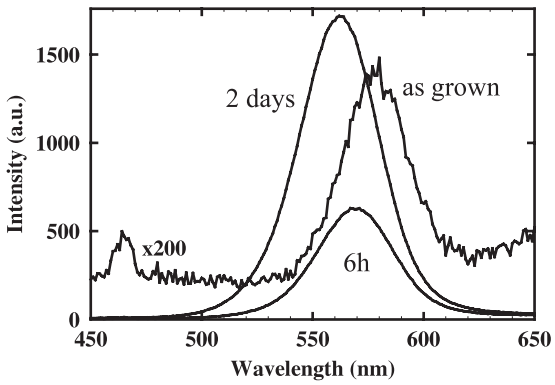

Figure 3. Photoactivation of a CdSe/silica composite. The parent solution contained 1.6×10^{-3} M cadmium perchlorate, 3.5×10^{-3} M sodium citrate and 4×10^{-4} M selenourea. Samples were photoactivated for the indicated times with a black light with a power of 15 W. Samples were excited with 400 nm light.

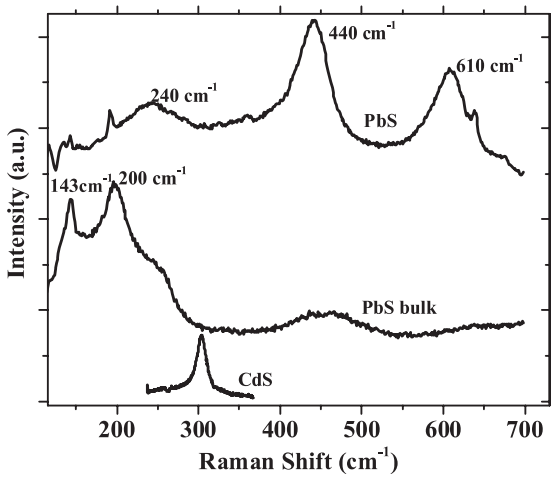

Figure 4. Room-temperature Raman spectra of PbS and CdS produced by x-ray lithography in silica hydrogels and measured with lines at 785 nm and 514 nm, respectively. The Raman spectrum of a PbS powder is also shown for reference.

as-grown samples was very weak, but increased by more than 300 times with photoactivation. The emission maximum was around 580 nm before photoactivation, and around 560 nm at the end of the photoactivation period. The blue shift of the emission indicates that the mean size of the nanoparticles is reduced by photoactivation. Particle size reduction upon illumination has been reported also by other groups [14, 20, 21, 32] and is not surprising, since photoactivation removes atoms preferentially but not exclusively from surface defects. Luminescence quantum yields were determined with two different procedures, which are described in section 2. The quantum yields calculated with these procedures were quite consistent and indicated that the quantum yield of citrate-stabilized quantum dot composites could be increased to up to 30% [32]. This high value of the quantum yield is in substantial agreement with recent reports of photoactivation of quantum dots. For example, citrate-capped CdSe quantum dots can be photoactivated to reach a quantum yield as high as 59%. The quantum yield of our composites is comparable to or higher than the quantum yield of commercially available polymer/quantum dot composites [40], and to the quantum yield of recently reported latex spheres decorated with quantum dots and of photonic crystals (opals) infiltrated with quantum dots [47]. All these composites have a quantum yield on the order of 10% [48].

The chemical identity and the structure of the nanoparticles in the patterned regions were investigated in our previous reports using techniques such as Raman spectroscopy, transmission electron microscopy, x-ray diffraction, and x-ray photoelectron spectroscopy. All these techniques showed that the nanoparticles were free of contamination, and that they had a bulk crystalline structure. In this work, we characterized the nanoparticles using Raman spectroscopy, and the results were in agreement with our previous research [15–17]. Representative Raman spectra are shown in figure 4 for CdS and PbS patterns obtained with x-ray lithography. CdS patterns exhibited a peak at 303 cm^{-1}. This frequency is in good agreement with previous Raman measurements of CdS/silica composites, and corresponds to the first-order longitudinal optical (LO) phonon frequency of CdS [15–17, 49]. The interpretation of the Raman results for PbS is more complex. The LO phonon of crystalline PbS at ∼205 cm^{-1} in normal Raman scattering is forbidden. However, by using an excitation source close to the intergap energies allows the forbidden Raman bands through the Fröhlich interaction mechanism [50]. The Raman spectrum of bulk PbS contains mainly three peaks at 154, 204, and 454 cm^{-1} [51]. The 154 cm^{-1} peak is a combination of a transverse acoustic (TA) and a transverse optic (TO) phonon; the 204 cm^{-1} peak is the first-order LO phonon; and the 450 cm^{-1} peak is the first overtone of the LO phonon (2LO). Our Raman measurements from a PbS powder show the first-order LO phonon at 200 cm^{-1} and a peak at 143 cm^{-1}, which probably arises due to a combination of TA and TO phonons. The Raman spectrum from monoliths patterned with PbS shows the second- and the third-order LO phonon peaks at 440 and 610 cm^{-1}, respectively. Observation of overtones which are not detected in the bulk appears to be a common phenomenon in nanocrystals [49] and has been reported for PbS nanoparticles with a mean size of 1.5 nm [52]. The origin of the 240 cm^{-1} peak is still under investigation; this could be the first-order LO phonon, which has an enhanced peak position due to the size of the nanocrystal. In 2 nm PbS nanocrystals, for example, the forbidden LO phonon appears at 230 cm^{-1} [53]. We notice that a shoulder around 240 cm^{-1} is also evident in the spectra of the PbS powder.

4. Conclusion

In conclusion, we have demonstrated a method of generating quantum dots with photolithography, which has several important features. Quantum dots can be synthesized with UV and x-ray lithographies, which have a very high theoretical spatial resolution. The process is water-based and highly luminescent composites can be fabricated in a few steps. The quantum yield of the composites can be increased with photoactivation to up to 30%, which is comparable to the quantum yield of the best commercial quantum dot composites. The main drawback of the technique, at this point, is probably polydispersity, which was estimated to be around 50% from

the FWHM of the exciton peak in the absorption spectra. Polydispersity might be eliminated by using matrices with well-contolled pore size, or by size-selective photocorrosion, and this is where our research will focus in the near future.

Acknowledgments

We gratefully acknowledge discussions and technical help from professor Carlo Segre and Dr Vladimir Zyryanov. This work was partly supported by the US Department of Energy (DOE) grant number DE-FG07-04ID14592. Materials Research Collaborative Access Team (MRCAT) operations are supported by the Department of Energy and the MRCAT member institutions. Part of this work was carried out at the Center for Nanoscale Materials, Argonne National Laboratory under contract number (DE-AC02-06CH11357) between University of Chicago Argonne LLC and the Department of Energy.

References

[1] Tohge N, Asuka M and Minami T 1990 *Proc. SPIE, Sol–Gel Optics* **1328** 125
[2] Capoen B, Gacoin T, Nedelec J M, Turrell S and Bouazaoui M 2001 *J. Mater. Sci.* **36** 2565
[3] Gong H-M, Wang X-H, Du Y-M and Wang Q-Q 2006 *J. Chem. Phys.* **125** 024707
[4] Lin Y, Zhang J, Kumacheva E and Sargent E H 2004 *J. Mater. Sci.* **39** 993
[5] Coe S, Woo W-K, Bawendi M G and Bulovic V 2002 *Nature* **420** 800
[6] Bakueva L, Musikhin S, Hines M A, Chang T-W F, Tzolov M, Scholes G D and Sargent E H 2003 *Appl. Phys. Lett.* **82** 2895
[7] Walker G W, Sundar V C, Rudzinski C M, Wun A W, Bawendi M G and Nocera D G 2003 *Appl. Phys. Lett.* **83** 3555
[8] Chen Y and Rosenzweig Z 2002 *Anal. Chem.* **74** 5132
[9] Gattás-Asfura K M and Leblanc R M 2003 *Chem. Commun.* **21** 2684
[10] Sundar V C, Eisler H-J and Bawendi M G 2002 *Adv. Mater.* **14** 739
[11] Klimov V I, Mikhailovsky A A, Xu S, Malko A, Hollingsworth J A, Leatherdale C A, Eisler H-J and Bawendi M G 2004 *Science* **290** 314
[12] Schaller R D, Petruska M A and Klimov V I 2003 *J. Phys. Chem.* B **107** 13765
[13] Schmidt H K 1992 *Proc. SPIE* **1758** 396
[14] Torimoto T, Murakami S-Y, Sakuraoka M, Iwasaki K, Okazaki K-I, Shibayama T and Ohtani B 2006 *J. Phys. Chem.* B **110** 13314
[15] Bertino M F, Gadipalli R R, Story J G, Williams C G, Zhang G, Sotiriou-Leventis C, Tokuhiro A T, Guha S and Leventis N 2004 *Appl. Phys. Lett.* **85** 6007
[16] Gadipalli R R, Matrin L A, Heckman B, Story J G, Bertino M F, Fraundorf P, Guha S and Leventis N 2006 *J. Sol–Gel Sci. Technol.* **40** 101
[17] Bertino M F, Gadipalli R R, Martin L A, Story J G, Heckman B, Guha S and Leventis N 2006 *J. Sol–Gel Sci. Technol.* **39** 299
[18] Smith H I and Cerrina F 1997 *Microlithogr. World* **6** 10
[19] Kresge C T, Leonowicz M E, Roth W J, Vartuli J C and Beck J S 1992 *Nature* **359** 710
[20] Matsumoto H, Sakata T, Mori H and Yoneyama H 1996 *J. Phys. Chem.* **100** 13781
[21] Torimoto T, Kontani H, Shibutani Y, Kuwabata S, Sakata T, Mori H and Yoneyama H 2001 *J. Phys. Chem.* B **105** 6838
[22] Leventis N, Elder I A, Rolison D R, Anderson M L and Merzbacher C I 1999 *Chem. Mater.* **11** 2837
[23] Divan R, Mancini D C, Gallagher S M, Booske J and Van der Weide D 2004 Improvements in graphite-based x-ray mask fabrication for ultra-deep x-ray lithography *Microsyst. Technol.* **10** 728
[24] Wang C Y, Mo X, Zhou Y, Zhu Y R, Liu H T and Chen Z Y 2000 *J. Mater. Chem.* **10** 607
[25] Zhao W-B, Zhu J-J and Chen H-Y 2003 *J. Cryst. Growth* **252** 587
[26] Lin Y-W, Hsieh M-M, Liu C-P and Chang H-T 2005 *Langmuir* **21** 728
[27] Chena Y-W, Zhou X-L, Tong J, Truong Y and Belzile N 2005 *Anal. Chem. Acta* **545** 149
[28] Hayes D, Micic O I, Nenadovic M T, Swayambunathan V and Meisel D 1989 *J. Phys. Chem.* **93** 4603
[29] Mostafavi M, Liu Y P, Pernot P and Belloni J 2000 *Radiat. Phys. Chem.* **59** 49
[30] Bertino M F, Hund J F, Sosa J, Zhang G, Sotiriou-Leventis C, Leventis N, Tokuhiro A T and Terry J 2004 *J. Non-Cryst. Solids* **333** 108
[31] Wang Y, Tang Z, Correa-Duarte M A, Pastoriza-Santos I, Giersig M, Kotov N A and Liz-Marzan L M 2004 *J. Phys. Chem.* B **108** 15461
[32] Rogach A L, Kornowski A, Gao M, Eychmüller A and Weller H 1999 *J. Phys. Chem.* B **103** 3065
[33] Meissner D, Memming R and Kastening B 1988 *J. Phys. Chem.* **92** 3476
[34] Meissner D, Lauermann I, Memming R and Kastening B 1988 *J. Phys. Chem.* **92** 3484
[35] Bunker C E, Harruff B A, Pathak P, Payzant A, Allard L F and Sun Y-P 2004 *Langmuir* **20** 5642
[36] van Sark W G J H M, Frederix P L T M, Van den Heuvel D J, Gerritsen H C, Bol A A, van Lingen J N J, de Mello Donega C and Meijerink A 2001 *J. Phys. Chem.* B **105** 8281
[37] Kunets V P, Kulish N R, Lisitsa M P and Bryksa V P 2004 *Semiconductors* **38** 447
[38] Kloepfer J A, Bradforth S E and Nadeau J L 2005 *J. Phys. Chem.* B **109** 9996
[39] van Dijken A, Janssen A H, Smitsmans M H P, Vanmaekelbergh D and Meijerink A 1998 *Chem. Mater.* **10** 3513
[40] Winter J O, Gomez N, Gatzert S, Schmidt C E and Korgel B A 2005 *Colloids Surf.* A **254** 147
[41] Wang Y, Tang Z, Correa-Duarte M A, Liz-Marzan L M and Kotov N A 2003 *J. Am. Chem. Soc.* **125** 2830
[42] Jones M, Nedeljkovic J, Ellingson R J, Nozik A J and Rumbles G 2003 *J. Phys. Chem.* B. **107** 11346
[43] Cordero S R, Carson P J, Estabrook R A, Strouse G F and Buratto S K 2000 *J. Phys. Chem.* B **104** 12137
[44] Bol A A and Meijerink A 2001 *J. Phys. Chem.* B. **105** 10203
[45] Manna L, Scher E C, Li L-S and Alivisatos A P 2002 *J. Am. Chem. Soc.* **124** 7136
[46] Cao Y C and Wang J 2004 *J. Am. Chem. Soc.* **126** 14336
[47] Maskaly G R, Petruska M A, Nanda J, Bezel I V, Schaller R D, Htoon H, Pietryga J M and Klimov V I 2006 *Adv. Mater.* **18** 343
[48] Sheng W, Kim S, Lee J, Kim S-W, Jensen K and Bawendi M G 2006 *Langmuir* **22** 3782
[49] Rolo A G, Vieira L G, Gomes M J M, Ribeiro J L, Belsley M S and dos Santos M P 1998 *Thin Solid Films* **312** 348
[50] Reedyk M, Thomsen C, Cardona M, Xue J S and Greedan J E 1994 *Phys. Rev.* B **50** 13762
[51] Smith G D, Firth S, Clark R J H and Cardona M 2002 *J. Appl. Phys.* **92** 4375
[52] Krauss T D and Wise F W 1997 *Phys. Rev.* B **55** 9860
[53] Krauss T D, Wise F W and Tanner D B 1996 *Phys. Rev. Lett.* **76** 1376